Research Article
Hepatic and Biliary Cancer

JOURNAL
OF HEPATOLOGY

Uncoupling immune trajectories of response and adverse events from anti-PD-1 immunotherapy in hepatocellular carcinoma

Graphical abstract

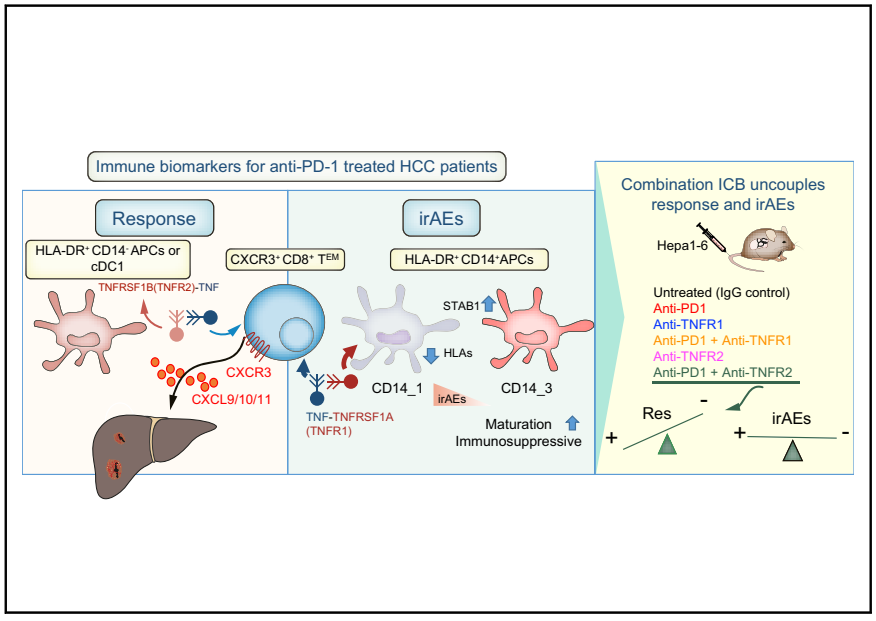

Highlights

- Distinct immune subsets are linked to response and toxicity in immunotherapy.
- Antigen-presenting cells and CD8 T_{EM} cell function act as an interface between response and toxicity.
- Diverging immune trajectories of immune subsets contribute to either response or toxicity.
- TNFR2 inhibition uncouples response and toxicity in anti-PD-1 immunotherapy.

Authors

Samuel Chuah, Joycelyn Lee, Yuan Song, …, Su Pin Choo, David Tai, Valerie Chew

Correspondence

david.tai.w.m@singhealth.com.sg (D. Tai), valerie.chew@duke-nus.edu.sg (V. Chew).

Lay summary

Response rates to immune checkpoint blockade (ICB) treatment in hepatocellular carcinoma (HCC) remain modest and adverse events are common. Herein, we identified early predictors of response and gained an in-depth understanding of the immunological mechanisms behind response and adverse events in patients with HCC treated with ICB. We also proposed a new combination immunotherapy for HCC that enhances response without exacerbating adverse events.

https://doi.org/10.1016/j.jhep.2022.03.039

Research Article
Hepatic and Biliary Cancer

JOURNAL OF HEPATOLOGY

Uncoupling immune trajectories of response and adverse events from anti-PD-1 immunotherapy in hepatocellular carcinoma

Samuel Chuah[1], Joycelyn Lee[2], Yuan Song[3], Hyung-Don Kim[4], Martin Wasser[1,5], Neslihan A. Kaya[6,7], Kyunghye Bang[4], Yong Joon Lee[8], Seung Hyuck Jeon[8], Sheena Suthen[1], Shamirah A'Azman[1], Gerald Gien[1], Chun Jye Lim[1], Camillus Chua[1], Sharifah Nur Hazirah[1], Hong Kai Lee[9], Jia Qi Lim[6], Tony K.H. Lim[5,10], Joe Yeong[5,10,11], Jinmiao Chen[9], Eui-Cheol Shin[8], Salvatore Albani[1,5], Weiwei Zhai[6,12,13], Changhoon Yoo[4], Haiyan Liu[3], Su Pin Choo[2,14], David Tai[2,*], Valerie Chew[1,5,*]

[1]*Translational Immunology Institute (TII), SingHealth-DukeNUS Academic Medical Centre, Singapore 169856, Singapore;* [2]*Division of Medical Oncology, National Cancer Centre Singapore, Singapore 169610, Singapore;* [3]*Immunology Programme, Life Sciences Institute, Immunology Translational Research Program and Department of Microbiology and Immunology, Yong Loo Lin School of Medicine, National University of Singapore, Singapore 117456, Singapore;* [4]*Department of Oncology, Asan Medical Center (AMC), University of Ulsan College of Medicine, 88, Olympic-ro 43-gil, Songpa-gu, Seoul 05505, Republic of Korea;* [5]*Duke-NUS Medical School, Singapore 169857, Singapore;* [6]*Genome Institute of Singapore (GIS), Agency for Science, Technology and Research (A*STAR), Singapore 138672, Singapore;* [7]*School of Biological Sciences, Nanyang Technological University, Singapore 637551, Singapore;* [8]*Graduate School of Medical Science and Engineering, Korea Advanced Institute of Science and Technology (KAIST), Daejeon 34141, Republic of Korea;* [9]*Singapore Immunology Network (SIgN), A*STAR, Singapore 138648, Singapore;* [10]*Department of Anatomical Pathology, Singapore General Hospital (SGH), Singapore 169856, Singapore;* [11]*Institute of Molecular and Cell Biology (IMCB), Agency for Science, Technology and Research (A*STAR), Singapore 138673, Singapore;* [12]*Key Laboratory of Zoological Systematics and Evolution, Institute of Zoology, Chinese Academy of Sciences, Beijing 100107, China;* [13]*Center for Excellence in Animal Evolution and Genetics, Chinese Academy of Sciences, Kunming 650223, China;* [14]*Curie Oncology, Mount Elizabeth Novena Specialist Centre, Singapore 329563, Singapore*

Background & Aims: While immune checkpoint blockade (ICB) has shown promise in patients with hepatocellular carcinoma (HCC), it is associated with modest response rates and immune-related adverse events (irAEs) are common. In this study, we aimed to decipher immune trajectories and mechanisms of response and/or irAEs in patients with HCC receiving anti-programmed cell death 1 (anti-PD-1) therapy.

Methods: Pre- and on-treatment peripheral blood samples (n = 60) obtained from 32 patients with HCC (Singapore cohort) were analysed by cytometry by time-of-flight and single-cell RNA sequencing, with flow cytometric validation in an independent Korean cohort (n = 29). Mechanistic validation was conducted by bulk RNA sequencing of 20 pre- and on-treatment tumour biopsies and using a murine HCC model treated with different immunotherapeutic combinations.

Results: Single-cell analyses identified $CXCR3^+CD8^+$ effector memory T (T_{EM}) cells and $CD11c^+$ antigen-presenting cells (APC) as associated with response (p = 0.0004 and 0.0255, respectively), progression-free survival (p = 0.00079 and 0.0015, respectively), and irAEs (p = 0.0034 and 0.0125, respectively) in anti-PD-1-treated patients with HCC. Type-1 conventional dendritic cells were identified as the specific APC associated with response, while 2 immunosuppressive $CD14^+$ myeloid clusters were linked to reduced irAEs. Further analyses of $CXCR3^+CD8^+$ T_{EM} cells showed cell-cell interactions specific to response *vs.* irAEs, from which the anti-PD-1 and anti-TNFR2 combination was harnessed to uncouple these effects, resulting in enhanced response without increased irAEs in a murine HCC model.

Conclusions: This study identifies early predictors of clinical response to anti-PD-1 ICB in patients with HCC and offers mechanistic insights into the immune trajectories of these immune subsets at the interface between response and toxicity. We also propose a new combination immunotherapy for HCC to enhance response without exacerbating irAEs.

Clinical trial number: NCT03695952.

Lay summary: Response rates to immune checkpoint blockade (ICB) treatment in hepatocellular carcinoma (HCC) remain modest and adverse events are common. Herein, we identified early predictors of response and gained an in-depth understanding of the immunological mechanisms behind response and adverse events in patients with HCC treated with ICB. We also proposed a new combination immunotherapy for HCC that enhances response without exacerbating adverse events.

Keywords: Checkpoint inhibitor; immunoprofiling; immune network; cellular cross-talk; liver cancer.

Received 9 November 2021; received in revised form 27 March 2022; accepted 31 March 2022; available online 15 April 2022

* Corresponding authors. Addresses: Division of Medical Oncology, National Cancer Centre Singapore, Singapore 169610, Singapore. (D. Tai), or Translational Immunology Institute (TII), SingHealth-DukeNUS Academic Medical Centre, Singapore 169856, Singapore. (V. Chew).

E-mail addresses: david.tai.w.m@singhealth.com.sg (D. Tai), valerie.chew@duke-nus.edu.sg (V. Chew).

https://doi.org/10.1016/j.jhep.2022.03.039

Introduction

Immune checkpoint blockade (ICB) by antibodies targeting molecules such as programmed cell death-1 (PD-1) and cytotoxic T lymphocyte-associated protein-4 (CTLA4) are among the most widely used cancer immunotherapies. ICB has achieved promising outcomes in various malignancies, including hepatocellular carcinoma (HCC), which remains the sixth-most common cancer and fourth leading cause of cancer mortality worldwide.[1] The use of anti-PD-1 ICB monotherapy in patients with advanced HCC produced modest objective response rates (ORRs) of 15% or 18.3% in phase III trials for nivolumab[2] and pembrolizumab,[3] respectively. In addition, about 20% of patients experienced grade 3 or higher treatment-induced immune-related adverse events (irAEs).[2,3] While recently reported combination immunotherapies for HCC conferred greater ORRs, irAEs increased in tandem. For instance, anti-PD-1 combined with anti-CTLA4 for patients with advanced HCC resulted in ORRs of 31% and grade 3/4 irAEs of 37% (CheckMate040),[4] and anti-programmed death-ligand 1 (PD-L1) combined with anti-vascular endothelial growth factor-A resulted in ORRs of 27.3% and grade 3/4 AEs of 56.5% (IMBRAVE150).[5] Therefore, a better understanding of the mechanisms of response and/or irAEs is critical for improving outcomes associated with ICB.

The development of single-cell, multi-parametric technologies has provided the means to extract valuable data from limited samples, enabling in-depth characterisation of the immune landscape for mechanistic and biomarker discovery.[6] Response to immunotherapy requires re-activation of the immunosuppressive tumour microenvironment (TME). Nonetheless, the systemic immune landscape plays an important role in the anti-tumour immune response[7] and provides a practical and minimally invasive source of biomarkers in the clinical setting. Moreover, irAEs that could be fatal and delay or disrupt treatment[8] commonly manifest as systemic autoimmune conditions.

In this study, we conducted deep single-cell immunoprofiling of patients with HCC to identify immune signatures predictive of response to anti-PD-1 therapy and to elucidate the mechanisms behind response *vs.* irAEs.

Materials and methods

Patient samples

Patients with HCC receiving anti-PD-1 ICB – nivolumab or pembrolizumab from the National Cancer Centre, Singapore (SG cohort n = 32, Table S1, real-world clinical cohort) or nivolumab from the Asan Medical Center, South Korea (KR cohort n = 29, Table S2, NCT03695952) – who provided written informed consent were recruited according to the Institutional Review Board guidelines of each institution. Patients received intravenous nivolumab (3 mg/kg) every 2 weeks or pembrolizumab (200 mg) every 3 weeks. Blood samples were collected at baseline (both cohorts) and during treatment (SG cohort only). Treatment response was monitored using RECIST1.1 and irAEs were assessed using National Cancer Institute Common Terminology Criteria for Adverse Events (NCI CTCAE; version 4.03). Peripheral blood mononuclear cells (PBMCs) were isolated using Ficoll-Paque Plus (GE Healthcare, UK) (SG Cohort) or Lymphocyte Separation Medium (Corning) (KR cohort). mRNA from pre and 1-week on-treatment tumour biopsies were obtained (n = 10 patients, SG cohort).

HCC model

Male C57BL/6 mice (aged 6–8 weeks; InVivos, Singapore), housed in specific pathogen-free conditions according to guidelines of Institutional Laboratory Animal Care and Use Committee of the National University of Singapore, were inoculated with 1×10^6 Hepa1-6 murine hepatoma cells via hydrodynamic tail-vein injection.[9] From day 7, tumour-bearing mice were injected intraperitoneally bi-weekly for 2 weeks with anti-PD-1 (RMP1-14, 250 μg/mouse), anti-TNFR1 (55R-170, 250 μg/mouse), anti-TNFR2 (TR75-54.7, 500 μg/mouse), alone or in combination (anti-PD1+anti-TNFR1, anti-PD1+anti-TNFR2), Armenian hamster IgG (PIP, 500 μg/mouse) and rat IgG2a (1-1, 250 μg/mouse) (all from ichorbio, UK). On day 21, mice were euthanized by CO_2 asphyxiation and the numbers of liver tumour nodules and liver weights were recorded. Infiltrating leucocytes from tumour and non-tumour liver tissue were isolated for flow cytometry analysis. Mouse colons were flushed and collected for formalin-fixed paraffin embedding using the Swiss-rolling method.

Cytometry by time-of-flight

Cytometry by time-of-flight (CyTOF) staining was performed as previously described[10] with a panel of 39 antibodies (Table S3) and analysed using a Helios mass cytometer (Fluidigm, USA). Data were down-sampled to 10,000 viable $CD45^+$ cells for in-house developed Extended Poly-dimensional Immunome Characterisation.[11] Clustering was performed with the FlowSOM algorithm, dimension reduction by t-distributed stochastic neighbour embedding, and visualisation with the R shiny app 'SciAtlasMiner'. Enriched clusters were identified by 2-tailed Mann-Whitney *U* test and validated with manual gating using FlowJo (V.10.5.2; FlowJo, USA).

Flow cytometry

Baseline PBMC samples from 29 patients (KR cohort) were stained with 13 antibodies (Table S4) and analysed using a BD LSR II cytometer. Immune cells from mouse samples were stained with 10 antibodies (Table S5). The Intracellular Fixation/Permeabilization Buffer Set (eBioscience) was used for intracellular staining. All data analysis was conducted using FlowJo V.10.5.2.

Single-cell RNA sequencing

Single-cell RNA sequencing (scRNA-seq) was performed on 10 PBMC samples consisting of 9 on-treatment samples (6 Res *vs.* 3 Non-Res; 5 Tox *vs.* 4 Non-Tox) and 1 matched pre-treatment sample (HCC6; Res/Tox) (Table S1). The 5' gene expression libraries were prepared using the 10x Genomics platform for indexed paired-end sequencing of 2x150 base pairs on an Illumina HiSeq 4000 system at 20,000 read pairs per cell. Reads were aligned to the human GRCh38 reference genome and quantified using cellranger count (10x Genomics, v3.0.2). Data repository ID: EGAS00001004843. Cells with <200 genes and >10% mitochondrial RNA were filtered, followed by analyses using Seurat (v3.0) pipelines. A total of 29 cell clusters were annotated based on the expression of known cell lineage-specific genes (Table S6).

Functional pathway analysis was conducted using Database for Annotation, Visualization and Integrated Discovery (DAVID) v6.8. CellPhoneDB 2.0[12] was used to analyse ligand-receptor expression and predict cell-cell communications of CXCR3-expressing CD8 T cells using default parameters.

Bulk RNA-seq

mRNA from matched pre- and 1-week on-treatment tumour biopsies (n = 10 patients, Table S1) were obtained using the Qiagen AllPrep DNA/RNA Mini Kit and sequenced using HiSeq 4000 platform. Raw reads were aligned to the Human Reference Genome hg19 via STAR and the expected gene-level counts were calculated using RSEM. Protein-coding genes with >0.5 counts per million were retained and differentially expressed gene (DEG) analyses were conducted using R package DESeq2 with Benjamini-adjusted p <0.05 and $|\log_2(\text{fold-change})|>0.5$ (Table S7). Functional pathway analysis was conducted using DAVID v6.8.

Statistical analysis

Statistical analyses were performed using unpaired Mann-Whitney U or Wilcoxon matched-pairs tests with 2-tailed p values using GraphPad Prism7. Cox regression with Wald test analysis and Kaplan-Meier curves with Log-rank tests were performed using the R package survminer.

Results

Early immunological predictors of response in the peripheral blood

Pre- and on-treatment blood samples from patients with HCC receiving anti-PD-1 ICB (SG cohort: n = 32; Table S1) were analysed using CyTOF and scRNA-seq to uncover the mechanisms of response and irAEs (Fig. 1A). An additional KR cohort (n = 29; Table S2) was included as a validation cohort and analysed using flow cytometry for defined biomarkers identified from the SG cohort. Further validation was conducted by bulk RNA-seq analysis of pre-*vs.* 1-week on-treatment tumour biopsies (SG cohort) and using a murine HCC model (Fig. 1A). The patients were stratified as: responders (Res), those who showed partial response or stable disease for ≥6 months; and non-responders (Non-Res), those who showed progressive disease within 6 months according to RECIST1.1. The 6-month time-point was identified from the Checkmate040 study, in which disease control with stable disease for ≥6 months was reported in 37% of patients with HCC treated with nivolumab.[13] Patients were also categorised as: Tox, those who experienced Grade (G) 2 and above irAEs; and Non-Tox, those with G1 or no irAEs according to NCI CTCAE v4.03, where G2 irAEs is the point where therapeutic interventions or ICB interruption would be considered.[8]

CyTOF analysis[11] revealed clusters corresponding to major immune lineages and subtypes according to the relative expression of 38 immune markers (Fig. S1A,B). To identify biomarkers for early prediction of response, we selected pre- and early on-treatment samples (<6 weeks from treatment initiation, before the first restaging CT scan for efficacy determination) from the SG cohort (n = 21; Table S1). The initial unsupervised Mann-Whitney U analysis of 6 Res *vs.* 6 Non-Res clinically matched samples (Table S1) revealed 2 $CD4^+$ clusters – namely, $FoxP3^+CD4^+$ T cells (C33) and $FoxP3^+CTLA4^+CD4^+$ regulatory T cells (Tregs) (C3), and a $CD8^+CD45RO^+CCR7^-CXCR3^+$ T_{EM} (C76) cluster – that were enriched in Res (Fig. 1B,C and S1C). Two distinct $CD11c^+$ myeloid cell clusters, C4 ($HLADR^{hi}CD86^+$ – indicative of antigen presentation capabilities) and C37 ($CD14^+HLADR^{lo/-}$ – potentially myeloid-derived suppressor cells[14]) were enriched in Res and Non-Res, respectively (Fig. 1B,C and S1C). Validation of these clusters by supervised manual gating with FlowJo (Fig. S2A) confirmed the significant enrichment of these immune subsets (n = 21, Fig. 1D). Notably, these clusters showed similar frequencies in pre- or early on-treatment (<6 weeks) blood, particularly in Res (Fig. S2B).

We next validated the enrichment of peripheral Tregs, $CXCR3^+CD8^+$ T_{EM} cells and APCs in Res, and myeloid-derived suppressor cells in Non-Res by flow cytometric analysis of an independent anti-PD1-treated KR cohort (n = 29; Fig. 1E, S3A and Table S2). Moreover, Kaplan-Meier analyses showed that higher frequencies of Tregs, APCs and $CXCR3^+CD8^+$ T_{EM} cells were significantly associated with superior progression-free survival (PFS) in both cohorts (Fig. 1F). Multivariate analyses of these biomarkers with clinical parameters revealed enrichment of $CXCR3^+CD8^+$ T_{EM} cells and APCs as independent predictors of PFS in both cohorts, while (≥G2) irAE incidence showed marginal significance (Table S8). To examine the influence of irAE status on the association of these immune biomarkers with response, we analysed them by segregating the patients according to their Tox status. We observed that $CXCR3^+CD8^+$ T_{EM} cells and APCs remained significantly enriched in Res, particularly in Non-Tox patients, from both cohorts (Fig. S2C and S3B). These data show that peripheral $CXCR3^+CD8^+$ T_{EM} cells and APCs are independent predictors of response and PFS in patients with HCC treated with anti-PD-1 ICB.

Peripheral immune markers associated with irAEs

Next, we analysed blood samples obtained during or close to (±2-weeks) ≥G2 irAEs (Tox) *vs.* those at matched post-ICB timepoints from patients who developed no or G1 irAEs (Non-Tox) (Table S1). Due to differences in the study design, this analysis was only performed for the SG cohort. Two $CXCR3^+CD38^+CD16^+CD56^+$ natural killer cell clusters (C89 and 99) showed enrichment in Tox (Fig. 2A,B and S4A). Conversely, 3 $CD8^+$ clusters – namely, C66 and C76 T_{EM} ($CD45RO^+CCR7^-$) cells and C96 ($V\alpha7.2^+CD161^+CD56^+CD8^+$) mucosal-associated invariant T cells – and a $CD11c^+CD14^+HLADR^+$ APC cluster (C27) were enriched in Non-Tox (Fig. 2A,B and S4A). Interestingly, the same $CXCR3^+CD8^+$ T_{EM} (C76) cluster was also enriched in Res as described earlier (Fig. S1C). Manual gating confirmed their enrichment (Fig. 2C and S4B). All 5 immune subsets displayed similar trends after controlling for response status (Fig. S4C). Thus, these immune subsets provide insights into irAE manifestation, regardless of their response status.

Distinct $CD11c^+$ myeloid APC subsets involved in response and irAEs

To obtain deeper molecular and mechanistic insights into on-treatment transcriptomic perturbations in the immune subsets identified, we conducted scRNA-seq on 10 PBMC samples consisting of 9 on-treatment PBMCs (6 Res *vs.* 3 Non-Res; 5 Tox *vs.* 4 Non-Tox) and 1 matched pre-treatment sample (Res/Tox) (Table S1). From 59,980 single cells, 29 clusters were identified and annotated according to their respective DEGs (Fig. 3A,B and Table S6).

Tregs (*CD3D*$^+$*CD4*$^+$*FOXP3*$^+$*CTLA4*$^+$*IL2RA*$^+$) and an APC cluster expressing *ITGAX* (CD11c), *HLA-DPA1, THBD* (CD141), and *CLEC9A,* representing type-1 conventional dendritic cells (cDC1),[15] were significantly enriched in Res (Fig. 3C,E and S5A,B). In addition, 2

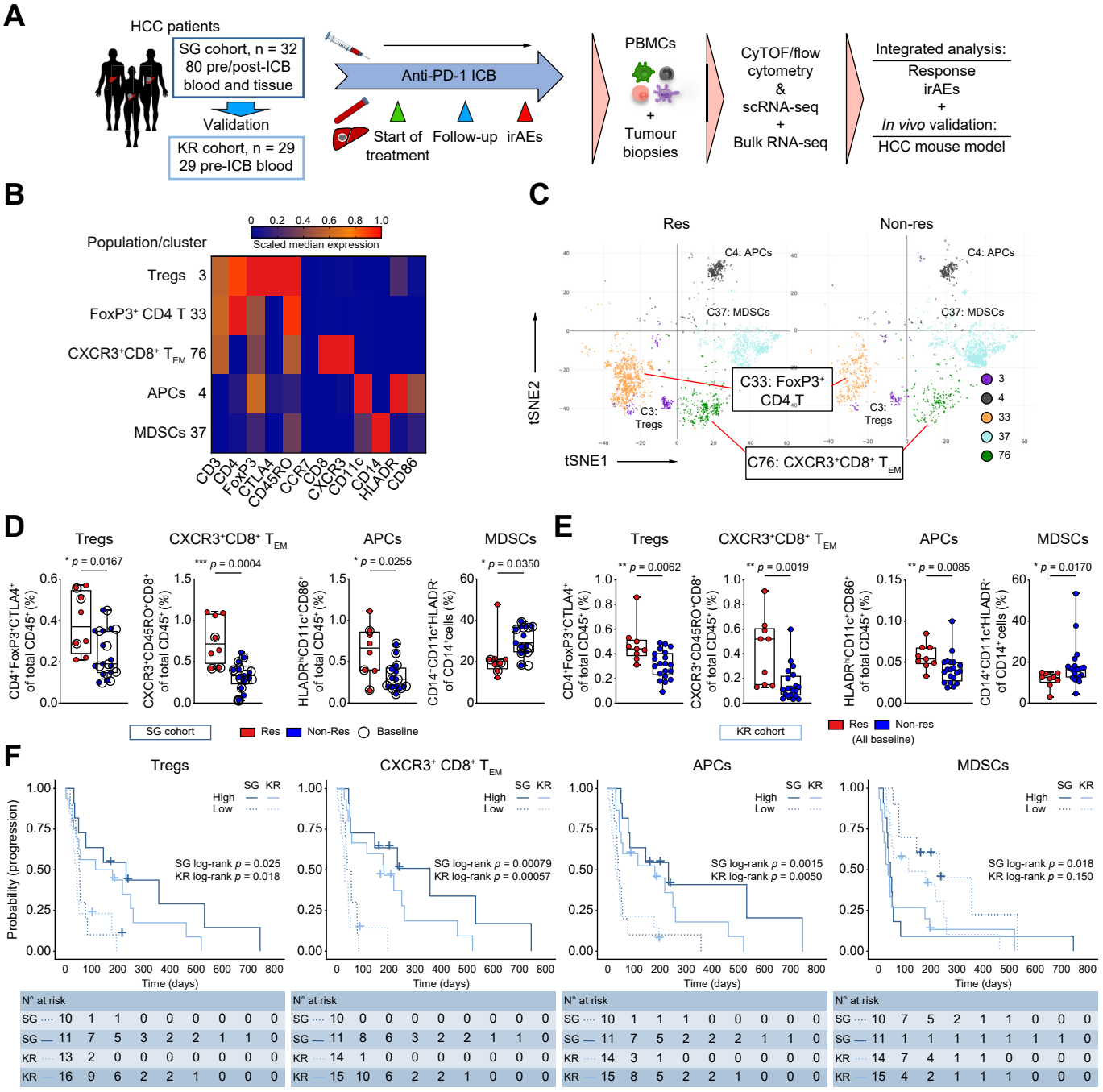

Fig. 1. Early peripheral predictors of response to anti-PD-1 immunotherapy. (A) Schematic illustration of clinical study design and data analysis. (B) Heatmap showing scaled median expression of key markers in the immune clusters enriched in Res or Non-Res. (C) tSNE plots showing enriched immune clusters (C) in Res or Non-Res. (D,E) Boxplots showing manually gated immune subsets in (D) Res (n = 8) or non-Res (n = 13) from SG cohort; and (E) Res (n = 9) or Non-Res (n = 20) from KR cohort. Median and interquartile range shown. Baseline samples indicated as black circles. *, ** denote 2-tailed p <0.05 and p <0.01, respectively, by unpaired Mann-Whitney U test. (F) Kaplan-Meier graphs showing PFS profiles of SG (n = 21) and KR cohorts (n = 29). Log-rank test p values are shown. APC, antigen-presenting cell; CyTOF, cytometry by time-of-flight; HCC, hepatocellular carcinoma; ICB, immune checkpoint blockade; irAEs, immune-related adverse events; KR, South Korea; MDSCs, myeloid-derived suppressor cells; Non-Res, non-responders; PBMCs, peripheral blood mononuclear cells; PFS, progression-free survival; Res, responders; scRNA-seq, single-cell RNA sequencing; SG, Singapore; T_{EM}, effector memory T; Tregs, regulatory T cells; tSNE, t-distributed stochastic neighbour embedding.

CD14 and *ITGAX* (CD11c)-expressing myeloid clusters, CD14-1 and CD14-3, were associated with Non-Tox (Fig. 3D,E and S5A,C). These CD14$^+$ clusters expressed higher levels of *KLF4* and *CLEC7A*, indicating potential polarization to immunosuppressive macrophages.[16,17]

To decipher the immune mechanisms behind the distinct clinical fates of response and irAEs, we next focused on CD11c$^+$ APCs which were associated with both events. The cDC1 cluster enriched in Res expressed the highest level of *HLA* genes (Fig. 3E and S5A), suggesting superior antigen presentation capability.

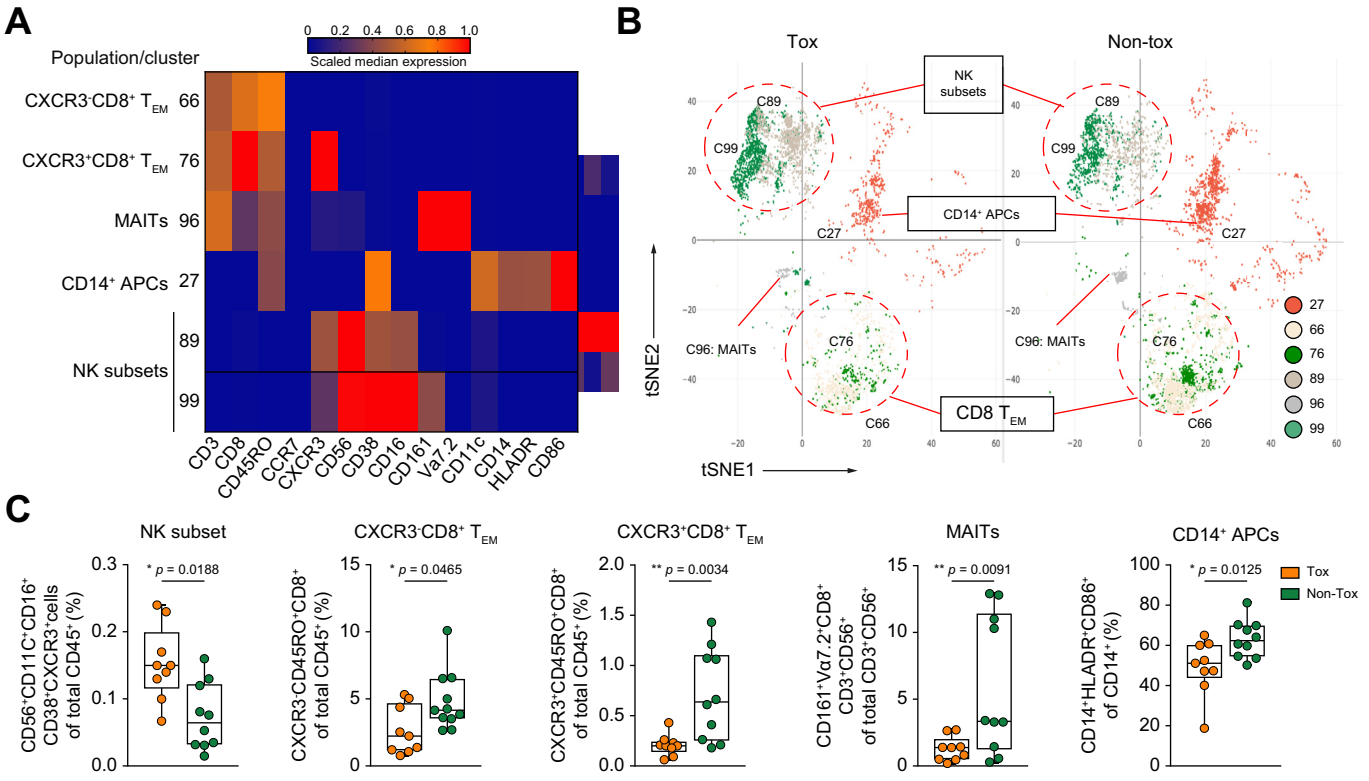

Fig. 2. Peripheral immune markers associated with irAEs. (A) Heatmap showing scaled median expression of key markers in the immune clusters enriched in either Tox (≥Grade 2 irAEs) or Non-Tox (Grade 1 or no irAEs). (B) tSNE plots showing enriched immune clusters (C) in Tox or Non-Tox. (C) Boxplots showing manually gated immune subsets in Tox (n = 9) or Non-Tox (n = 11). Median and interquartile range shown. *, **denote 2-tailed p <0.05 and p <0.01, respectively, by unpaired Mann-Whitney U test. APC, antigen-presenting cells; irAEs, immune-related adverse events; MAITs, mucosal invariant T cells; NK, natural killer; Non-Tox, non-toxicity; T_{EM}, effector memory T; Tox, toxicity; tSNE, t-distributed stochastic neighbour embedding.

Indeed, its enriched functional pathways included antigen processing and presentation via MHC class II, T-cell co-stimulation, and IFNγ-mediated signalling (Fig. 3F), which are important for immune priming. This corroborates other studies associating cDC1s with better survival in cancers, as well as with anti-tumour roles in adoptive T-cell therapy and ICB.[18]

Comparison of the other 2 myeloid clusters associated with non-Tox (CD14-1 and CD14-3) revealed that CD14-1 expressed higher levels of antigen-presenting *HLA*-related genes than CD14-3 (Fig. 3E and S5A, albeit lower than the cDC1 cluster). Conversely, CD14-3 expressed higher levels of immunosuppressive *STAB1* (Clever-1)[19] (Fig. 3E). Furthermore, among their enriched functional pathways, peptide antigen assembly with MHC class II and the pro-inflammatory IL-1β pathway were enriched in CD14-1 but not in CD14-3 (Fig. 3G). In summary, among these CD14 clusters, CD14-3, that is more significantly associated with Non-Tox (Fig. 3D), displayed reduced antigen presentation/inflammatory characteristics and a more immunosuppressive phenotype than CD14-1.

Distinct phenotypes of CXCR3⁺CD8⁺ T_{EM} cells in response and irAEs

Since we identified CXCR3⁺CD8⁺ T_{EM} cells as the immune subset common to both Res (Fig. 1D,E) and Tox (Fig. 2C), we next focused on *CXCR3*-expressing CD8 T cells (n = 863 cells) in the scRNA-seq data (Fig. S5D). Compared to all other T cells, multiple genes involved in antigen presentation, *HLA*(s), inflammation, granzymes (*GZM*)s and proliferation (*MKI67*) were enriched in the *CXCR3⁺CD8⁺* T cells (Fig. 4A). Conversely, the expression of naïve T-cell markers like *CCR7*, *IL7R* and *LEF1* was downregulated (Fig. 4A), suggesting an effector memory phenotype. Enriched functional pathways included inflammatory response, cytolysis and antigen processing and presentation via MHC class II (Fig. 4B). Thus, these CXCR3⁺CD8⁺ T_{EM} cells display a more inflammatory and cytolytic phenotype compared to other T cells.

Given that the systemic immune landscape is a dynamic ecosystem of immune cell cross-talk that could affect their functions in immunity, we employed CellPhoneDB[12] to identify the expression of receptors and ligands in CXCR3⁺CD8⁺ T_{EM} cells and predict their potential interactions with other immune cells. Lymphotoxin alpha and its receptors, tumour necrosis factor receptor superfamily (*TNFRSF*) *1A*, *1B* and lymphotoxin beta receptor, which could promote inflammation and oncogenesis,[20] were enriched in both Res and Tox (Fig. 4C,D). This suggests that CXCR3⁺CD8⁺ T_{EM} cells form pro-inflammatory interactions with other cells, leading to both response and irAEs.

Furthermore, we observed distinct *TNF* interactions between CXCR3⁺CD8⁺ T_{EM} and myeloid cell populations, where *TNF-TNFRSF1B* (TNFR2) was enriched in Res, but *TNF-TNFRSF1A* (TNFR1) was enriched in Non-Tox (Fig. 4C,D). The interactions of *TNF* with *TNFRSF1A* and *1B* play important roles in macrophage activation and inflammation.[21] To validate the protein expression of TNFα, TNFR1 and TNFR2, we performed flow cytometry on PBMCs from ICB-treated patients with HCC (Fig. S6A). Consistent with data shown in Fig. 4C, we found that TNFα expression was significantly higher particularly in CXCR3⁺CD8⁺ T_{EM} cells from

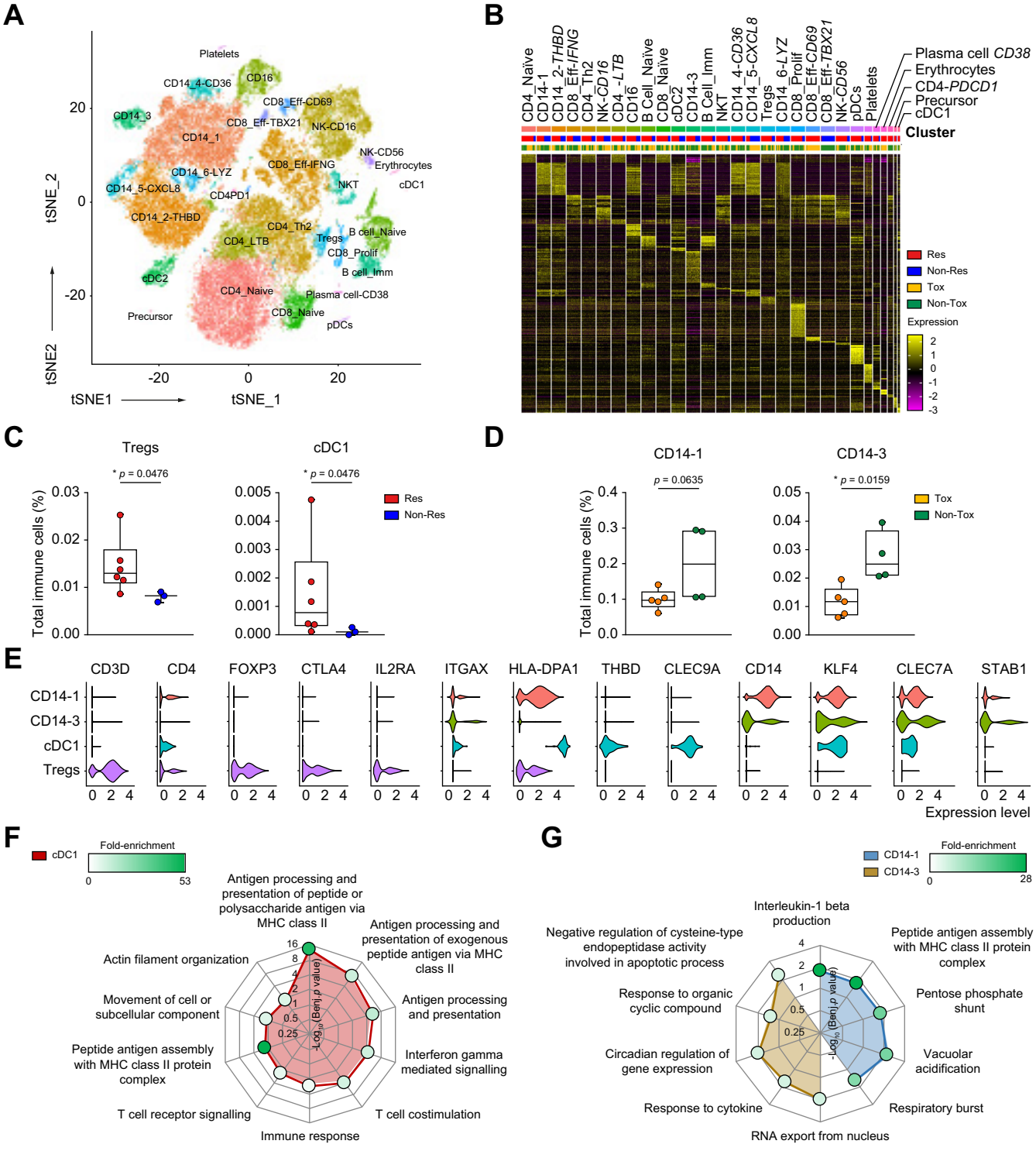

Fig. 3. scRNA-seq analysis of immune subsets associated with response and irAEs. (A) tSNE plot showing 29 scRNA-seq clusters. (B) Heatmap illustrating the top 10% DEGs of 29 clusters. (C,D) Box plots showing cell clusters enriched in Res (n = 6) or Non-Res (n = 3) and Tox (n = 5) or Non-Tox (n = 4). Median and interquartile range shown. *denotes 2-tailed p <0.05 by unpaired Mann-Whitney U test. (E) Violin plots of selected DEGs from the 4 enriched immune subsets in either response or irAEs. (F) Top 10 significant pathways by fold-enrichment for cDC1. (G) Top 5 significant pathways by fold-enrichment for both CD14-1 and CD14-3. (F,G) Vertical axis represents -$\log_{10}$(Benjamini)-adjusted p values and colour gradient represents fold-enrichment of each pathway. cDC, conventional dendritic cells; DEGs, differentially expressed genes; Eff, effector; Imm, immature; irAEs, immune-related adverse events; Non-Res, non-responders; Non-Tox, non-toxicity; pDCs, plasmacytoid DCs; Prolif, proliferative; Res, responders; Th2, T-helper 2 cells; Tox, toxicity; Tregs, regulatory T cells; tSNE, t-distributed stochastic neighbour embedding.

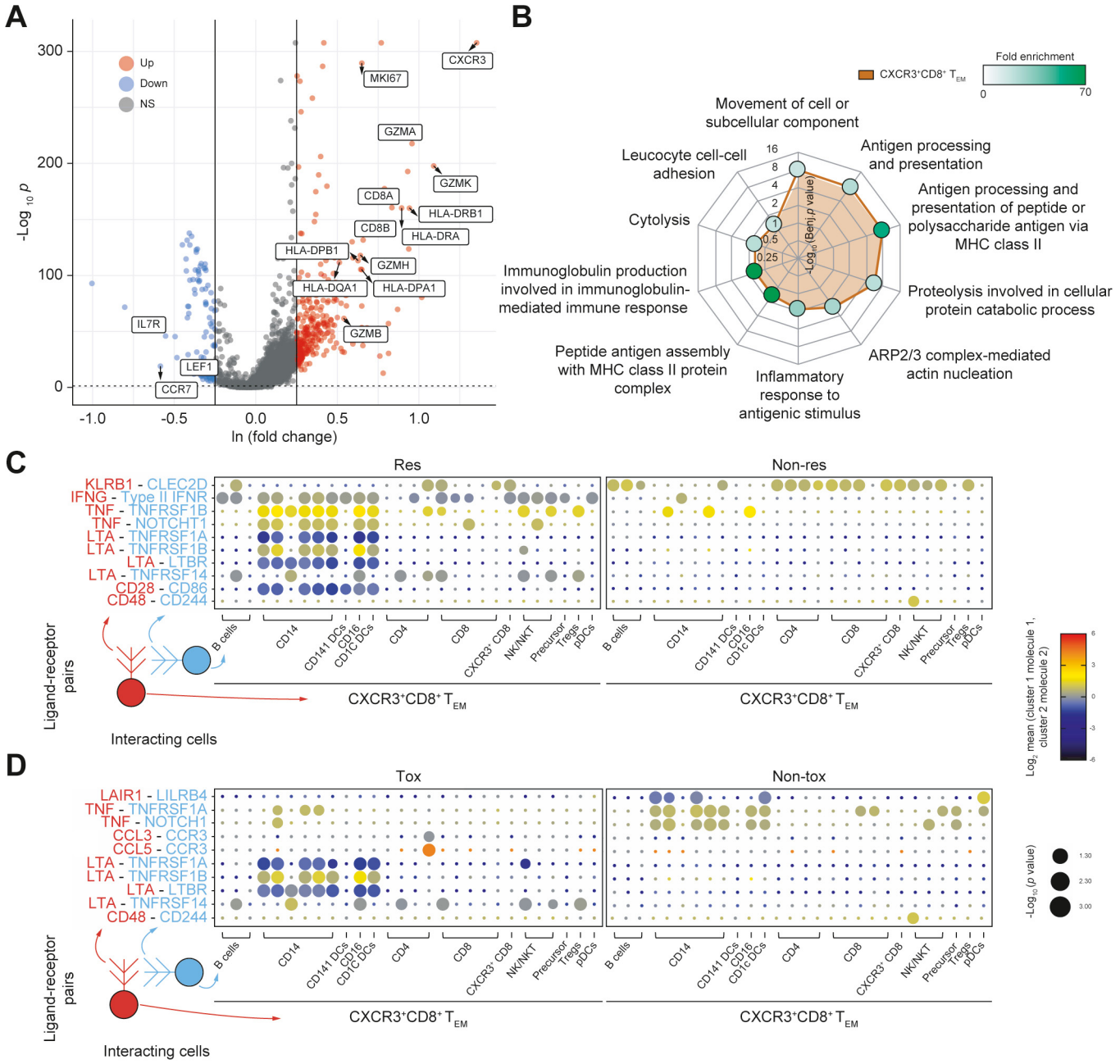

Fig. 4. CXCR3$^+$CD8$^+$ T_{EM} cells are involved in both response and irAEs. (A) Volcano plot showing DEGs comparing CXCR3$^+$CD8$^+$ T_{EM} against all T cells. Selected genes are highlighted in boxes as upregulated (Up): p <0.05 & ln(FC)>0.25, downregulated (Down): p <0.05 & ln(FC)<-0.25 or non-significant (n.s.): ln(fold-change)<±0.25. (B) Top 10 significantly enriched functional pathways from DEGs in CXCR3$^+$CD8$^+$ T_{EM} cells. Vertical axis represents the -$\log_{10}$(Benjamini) adjusted p values and colour gradient represents fold-enrichment. (C,D) Dot plots of selected ligand-receptor interacting pairs between CXCR3$^+$CD8$^+$ T_{EM} cells and all other immune clusters computed using CellPhoneDB in (C) Res/Non-Res and (D) Tox/Non-Tox. Point shade reflects $\log_2$Mean of average expression levels of interacting molecule 1 from cluster 1 and interacting molecule 2 from cluster 2. Point size indicates the -$\log_{10}$(p value). DEGs, differentially expressed genes; irAEs, immune-related adverse events; NK, natural killer; Non-Res, non-responders; Non-Tox, non-toxicity; pDCs, plasmacytoid DCs; Res, responders; T_{EM}, effector memory T; Tox, toxicity; Tregs, regulatory T cells; tSNE, t-distributed stochastic neighbour embedding.

Res than Non-Res (Fig. S6B). We also observed increased expression of TNFR1 on both CD14$^+$ monocytes and CD14$^-$CD11c$^+$HLA-DR$^+$ dendritic cells in Non-Tox *vs.* Tox (Fig. S6C). However, there was no significant difference in TNFR2 expression on monocytes and dendritic cells between Res and Non-Res or Tox and Non-Tox (Fig. S6D), indicating that the increased *TNF* interaction in Res (Fig. 4C) is largely driven by TNFα upregulation; while in Non-Tox (Fig. 4D), it is primarily due to increased TNFR1 expression. This suggests that the different TNF signalling pathways could be harnessed to uncouple response and irAEs in ICB.

Tissue recruitment of APCs and CXCR3$^+$CD8$^+$ T_{EM} cells

The trafficking of immune cells into tumour tissue, as part of the anti-tumour response induced by immunotherapy, could be reflected by changes in their frequencies in the blood.[22] We

compared the frequency of the response-associated immune subsets (Fig. 1D,E) and found a significant reduction in APCs and CXCR3$^+$CD8$^+$ T_{EM} cells in late (>10 weeks) compared to the matched early (<6 weeks) on-therapy blood samples (Table S1), indicating their tumour recruitment in Res (Fig. 5A) but not in Non-Res (Fig. S7A).

To link our observations in the blood to events in the TME, we conducted bulk tissue RNA-seq on pre- and 1 week on-treatment tumour biopsies from 10 ICB-treated patients with HCC (6 Res, 4 Non-Res) (Table S1). DEG analysis comparing on- *vs.* pre-treatment tumours from Res (Table S7) revealed upregulation of genes related to T-cell activation (*GZMA*, *GZMH*) and antigen presentation (*HLA*-related genes) (Fig. 5B), the same genes that were also upregulated in CXCR3$^+$CD8$^+$ T_{EM} cells and APCs (Fig. 4A and S5A). On-treatment enriched functional pathways from Res included antigen presentation, T-cell co-stimulation, leukocyte chemotaxis, and IFNγ-mediated signalling (Fig. 5C), many of which were again common functional pathways enriched in both

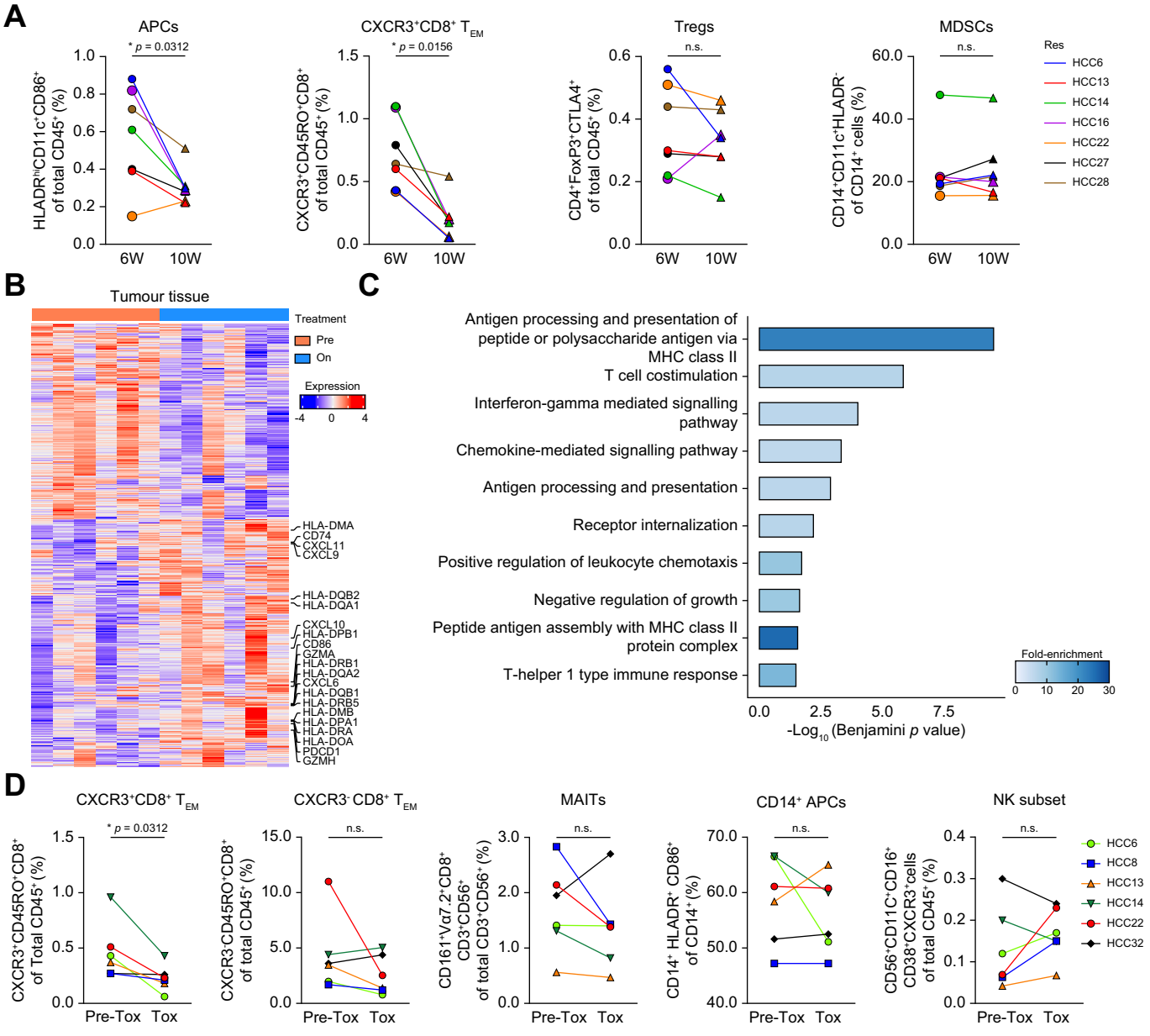

Fig. 5. Tissue recruitment of APCs and CXCR3$^+$CD8$^+$ T_{EM} cells upon immunotherapy. (A) Analyses of immune subsets from responders' matched PBMCs taken from early, <6 weeks (6W) *vs.* late, >10 weeks (10W) timepoints after anti-PD-1 treatment (n = 7); * denotes p <0.05; NS denotes non-significant 2-tailed p values by Wilcoxon signed-rank test. (B) Heatmap showing DEGs comparing pre-*vs.* on-treatment matched tumour tissues in responders to immunotherapy (n = 6). Selected DEGs of interest are highlighted. (C) Top 10 significantly enriched functional pathways of upregulated DEGs in matched on-treatment *vs.* pre-treatment tumour tissues from the responders. Horizontal-axis represents the -$\log_{10}$(Benjamini) adjusted p value and colour gradient represents enrichment fold. (D) Analyses of immune subsets from matched PBMCs taken before (Pre-Tox) and at the point of irAE manifestation (Tox) after anti-PD-1 treatment (n = 6); * and n.s. denotes p <0.05 or non-significant 2-tailed p values by Wilcoxon signed-rank test. APCs, antigen-presenting cells; DEGs, differentially expressed genes; irAE, immune-related adverse event; MAITs, mucosal invariant T cells; MDSCs, myeloid-derived suppressor cells; NK, natural killer; PBMCs, peripheral blood mononuclear cells; T_{EM}, effector memory T; Tox, toxicity; Tregs, regulatory T cells.

cDC1 and CXCR3$^+$CD8$^+$ T_{EM} cells (Fig. 3F, 4B); suggesting that these immune cells are recruited to the tumour tissue following ICB, particularly in Res. Moreover, it was intriguing to note the enrichment of *CXCL9*, *CXCL10* and *CXCL11* in Res (Fig. 5B), the key chemokines that bind to CXCR3, further supporting tumour recruitment of CXCR3$^+$CD8$^+$ T_{EM} cells in Res. In contrast, Non-Res showed a completely different set of DEGs that were unrelated to immune activation (Fig. S7B).

Since depletion of CXCR3$^+$CD8$^+$ T_{EM} cells was also related to irAEs (Fig. 2C), we compared their frequencies in matched on-treatment blood samples taken before (Pre-Tox) and during or close to (±2 weeks) irAEs (Tox). We found that CXCR3$^+$CD8$^+$ T_{EM} cells were indeed significantly depleted at the point of Tox manifestation (Fig. 5D), suggesting their recruitment to the tissue. Once again, these data highlight the importance of CXCR3-mediated migration of CXCR3$^+$CD8$^+$ T_{EM} cells in the manifestation of response and irAEs.

TNFR2 inhibition uncouples response and toxicity to anti-PD-1 ICB

Finally, our scRNA-seq data demonstrated that distinct TNF signalling pathways related to Res and Non-Tox (Fig. 4C,D) could be harnessed to uncouple response and irAEs upon ICB. We investigated this in mice inoculated with hepatoma cells via hydrodynamic tail-vein injection[9] and treated with anti-PD-1 and/or anti-TNFR1 or anti-TNFR2, bi-weekly for 2 weeks starting from day 7 post-tumour induction (Fig. 6A).

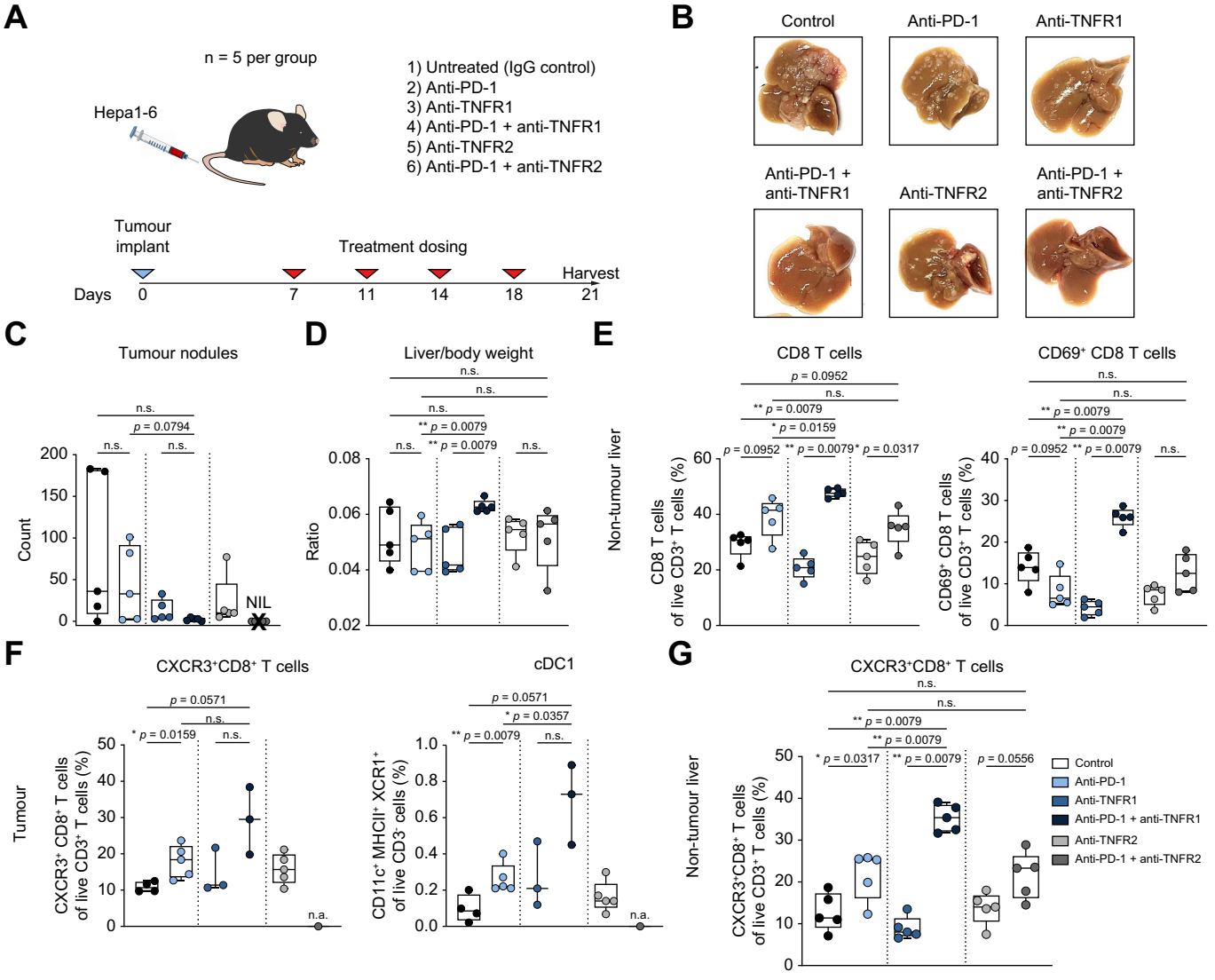

Fig. 6. Combination immunotherapies of anti-TNFR1 or anti-TNFR2 with anti-PD-1 in a murine HCC model. (A) Mice with HCC induced by hydrodynamic tail-vein injection of Hepa1-6 cells were randomly assigned to 6 treatment groups and treated bi-weekly for 2 weeks from day 7 to 21 (n = 5 mice per group). (B) Representative images of livers harvested from the mice at Day-21. (C) Tumour nodules from the mice. NIL, no tumours from all mice treated with anti-PD-1+anti-TNFR2. (D) Liver/body weight ratio of the mice from each condition. (E) Frequencies (%) of CD8 T cells and CD69$^+$ active CD8 T cells in non-tumour liver tissues of the mice. (F) Frequencies (%) of CXCR3$^+$CD8$^+$ T cells and CD11c$^+$MHCII$^+$XCR1$^+$ cDC1 cells in tumour tissues of the mice. NA, no tumours from anti-PD-1+anti-TNFR2 treatment group. (G) Frequencies (%) of CXCR3$^+$CD8$^+$ T cells and cDC1 cells in non-tumour liver tissues from the mice. (C–F) Boxplots show median and interquartile range. *, ** n.s. denote 2-tailed p <0.05, p <0.01 or non-significant p values by unpaired Mann-Whitney U test. cDC1, type 1 conventional dendritic cells; HCC, hepatocellular carcinoma.

At harvest on day 21, all mice receiving combination treatments showed significant reduction in tumour nodules, especially those treated with anti-PD-1+anti-TNFR2, which displayed no tumour burden (Fig. 6B,C). We also observed a significantly higher liver-to-body weight ratio in the mice treated with the anti-PD-1+anti-TNFR1 combination (Fig. 6D) with no significant differences in mouse body weight (Fig. S8A) and reduced tumour burden in this group (Fig. 6C), suggesting liver hypertrophy and inflammation. The higher TNFR1 expression observed in Non-Tox (Fig. 4D and S6C), indicating its role in preventing irAEs, corroborates the enhanced toxicity observed in mice treated with the anti-PD1+anti-TNFR1 combination. This is further supported by increased $CD8^+$ T-cell infiltration, especially of pro-inflammatory $CD69^+$ activated $CD8^+$ T cells, in the non-tumour liver tissue (Fig. 6E and S8B) and enhanced colonic $CD4^+$ T-cell infiltration, indicating colitis and intestinal inflammation[23] (Fig. S8C,D). Enhanced toxicity was not observed in the anti-PD-1+anti-TNFR2 combination, which displayed the greatest tumour control (Fig. 6C-E and S8C,D), further strengthening our hypothesis that the differential blockade of TNFR1 or TNFR2 combined with anti-PD-1 therapy can uncouple response and irAEs.

The selective enhanced response following TNFR2 inhibition could stem from the preferential expression of TNFR2 on highly immunosuppressive Tregs.[24] To validate this, we sorted Tregs and non-Tregs from PBMCs, adjacent non-tumour liver and tumour tissues from patients with HCC (Fig. S9A). We found significantly higher expression of *TNFRSF1B* (TNFR2), but not *TNFRS1A* (TNFR1) in Tregs compared to non-Tregs in tumour-infiltrating leucocytes (Fig. S9B). *TNFRSF1B* expression was also higher in Tregs from tumour-infiltrating leucocytes compared to Tregs from PBMCs or non-tumour liver-infiltrating leukocytes (Fig. S9B). These findings demonstrated the specificity of TNFR2 expression on Tregs from HCC tumours, which upon selective inhibition, could enhance anti-tumour response but not systemic toxicity.

Furthermore, we observed intratumoural enrichment of $CXCR3^+CD8^+$ T cells and $CD11c^+MHCII^+XCR1^+$ cDC1 in the mice treated with anti-PD-1, which was further enhanced by the anti-PD-1+anti-TNFR1 combination that corresponded to enhanced tumour control (Fig. 6F and S8B). This corroborates our human data that indicated the recruitment of these cells to tumours in Res (Fig. 5A-C). Notably, the anti-PD-1+anti-TNFR1 combination group, which displayed enhanced irAEs, also displayed a significantly higher infiltration of $CXCR3^+CD8^+$ T cells in the non-tumour liver tissue (Fig. 6G and S8B), again validating our observation that these cells are recruited to irAE sites (Fig. 5D).

Thus, using this model, we validated anti-PD-1 and anti-TNFR2 as a novel ICB combination strategy for HCC that results in superior responses without enhanced irAEs.

Discussion

Biomarkers of response to ICB have been explored previously in HCC,[25,26] including the tumour 4-gene inflammatory signature that predicts superior survival[27] as well as greater tumour biodiversity and vascular endothelial growth factor expression, which are associated with poorer outcomes.[28] PD-L1 expression has also been associated with superior response to anti-PD-1 ICB in HCC.[27] Here, we identified circulating $CXCR3^+CD8^+$ T_{EM} cells and $CD11c^+HLADR^{hi}$ APCs, which are potentially recruited to the TME upon treatment, as biomarkers for response to anti-PD-1 ICB in patients with HCC. In support to our findings, previous studies in melanoma and lung cancer suggested that peripheral biomarkers like $CD14^+$ classical monocytes and central memory-to-effector T-cell ratios were associated with favourable clinical outcomes following anti-PD-1 therapy.[29,30] A recent study also demonstrated that T-cell clones recruited to the tumour upon treatment dictate ICB response.[31]

While other studies explored biomarkers for ICB-induced irAEs, such as intratumoural T-cell activation or clonal expansion[32] and circulating B cells,[33] none have explored the immunological trajectories spanning both response and irAEs. In our current study, we found that $CXCR3^+CD8^+$ T_{EM} cells with tissue-recruitment capability contributed to both response and irAEs, and demonstrated that local tumour inflammatory cues, specifically the upregulation of the chemokine ligands CXCL9, 10 and 11 upon ICB, induce their recruitment. Our findings are further supported by a recent meta-analysis across several solid tumours, where *CD8A* and *CXCL9* were identified as predictors of response to ICB.[34]

Finally, based on predicted cell-cell communications between $CXCR3^+CD8^+$ T_{EM} cells and other immune cells, we found distinct pathways involving TNFR1 and TNFR2 that could be harnessed to uncouple response from irAEs in anti-PD-1 ICB therapy. The benefits of anti-TNF treatment in enhancing the efficacy of ICB through modulation of potential irAEs have recently been discussed.[35] However, our current data further demonstrated that TNFR1 and TNFR2 each govern distinct pathways underlying response and irAEs. The TNF-TNFR2 interaction was enriched in Res and was largely driven by the increased expression of TNFα on $CXCR3^+CD8^+$ T_{EM} rather than TNFR2. Moreover, TNFR2 inhibition was recently proposed as a novel immunotherapeutic strategy that could confer enhanced anti-tumour efficacy due to the preferential expression of TNFR2 on highly immunosuppressive Tregs;[24] this hypothesis was validated in Tregs from HCC tumours in our current study. TNFR2 has also been implicated in immune evasion and tolerance,[36] making it a potential immune checkpoint target and a promising candidate for combination immunotherapy, as evidenced in our current HCC murine study.

Conversely, the TNF-TNFR1 interaction was enriched in Non-Tox in our study, indicating it may play an important role in preventing toxicity. Indeed, the enhanced toxicity observed following TNFR1 inhibition in our murine study is consistent with a previous study that linked TNFR1 inhibition to the expansion of pathogenic T-helper 1 and 17 pro-inflammatory cells in mice with collagen-induced arthritis.[37] Moreover, concerns over the use of broad-spectrum anti-TNF-α agents in autoimmune hepatitis[38] further emphasize the need to distinguish the underlying mechanisms of the TNFR1 and TNFR2 receptors in immunotherapy for HCC. The complex effects of these 2 receptors highlight the potential of selective TNFR2 inhibition as a promising immunotherapeutic strategy to uncouple anti-tumour efficacy from autoimmune toxicity in combination with anti-PD-1 ICB for HCC.

In conclusion, we identified early peripheral predictors of response in patients with HCC receiving anti-PD-1 therapy and provided valuable insights on the interface between response and irAEs, which could be harnessed to enhance clinical response without exacerbating the toxicity of HCC treatment.

Abbreviations

APC, antigen-presenting cell; cDC1, type-1 conventional dendritic cells; CTLA4, cytotoxic T lymphocyte-associated protein 4; CyTOF, cytometry by time-of-flight; DEGs, differentially expressed genes; G, grade; GZM, granzyme; HCC, hepatocellular carcinoma; ICB, immune checkpoint blockade; irAEs, immune-related adverse events; KR, South Korea; NCI CTCAE, National Cancer Institute Common Terminology Criteria for Adverse Events; Non-Res, non-responders; Non-Tox, non-toxicity; ORR, objective response rate; PBMCs, peripheral blood mononuclear cells; PD-1, programmed cell death 1; PD-L1, programmed death-ligand 1; PFS, progression-free survival; Res, responders; scRNA-seq, single-cell RNA sequencing; SG, Singapore; T_{EM}, effector memory T; TME, tumour microenvironment; TNF, tumour necrosis factor; TNFRSF, tumour necrosis factor receptor superfamily; Tox, toxicity; Treg, regulatory T cells.

Financial support

This work was supported by the National Medical Research Council (NMRC), Singapore (ref numbers: NMRC/OFLCG/003/2018, NMRC/TCR/015-NCC/2016, NMRC/CSA-SI/0013/2017, NMRC/CSA-SI/0018/2017 and NMRC/STaR/020/2013).

Conflict of interest

The authors declare no conflicts of interest that pertain to this work.

Please refer to the accompanying ICMJE disclosure forms for further details.

Authors' contributions

S. Chuah obtained and analysed data and prepared the paper. J. Lee recruited patients and involved in clinical study design. Y. Song performed the murine HCC work. H.D. Kim and K. Bang obtained and analysed clinical data from Korea cohort. M. Wasser performed CyTOF data analysis and discussed the data. N. Kaya analysed the tissue transcriptomic data and discussed the data. Y.J. Lee and S.H. Jeon were involved in sample collection and FACS data analysis of the Korea cohort. S.D/O. Suthen, S. A'Azman, G. Gien and C.J. Lim processed the samples and performed experiments. C. Chua, S. Hazirah, H.K. Lee and J.Q. Lim assisted in transcriptomic data collection and analysis. T.K.H. Lim and J. Yeong prepared and provided tissue samples and discussed the data. J.M. Chen assisted in scRNA-seq data analysis. E.C. Shin supervised and designed the FACS data analysis of the Korea cohort. S. Albani designed the CyTOF pipeline and discussed the data. W. Zhai collected and analysed the tissue transcriptomic data. C. Yoo recruited Korea cohort and discussed the data. H. Liu supervised and provided murine HCC data. S.P. Choo and D. Tai designed the clinical study, recruited patients and discussed the data. V. Chew designed and led the study, performed the analysis and prepared the paper.

Data availability statement

Raw scRNA-seq data has been deposited at the European Genome-phenome Archive (EGA) under accession number EGAS00001004843.

Acknowledgments

The authors would like to thank all participating patients, all members of TII, members of Dr. Chen Jinmiao's team from SIgN and the clinical research coordinators from NCCS and AMC for their contributions. Acknowledgement is also extended to Dr. Jessica Tamanini from Insight Editing London for scientific and language editing of this manuscript.

Supplementary data

Supplementary data to this article can be found online at https://doi.org/10.1016/j.jhep.2022.03.039.

References

Author names in bold designate shared co-first authorship

[1] Bray F, Ferlay J, Soerjomataram I, Siegel RL, Torre LA, Jemal A. Global cancer statistics 2018: GLOBOCAN estimates of incidence and mortality worldwide for 36 cancers in 185 countries. CA Cancer J Clin 2018;68:394–424.

[2] Yau T, Park JW, Finn RS, Cheng AL, Mathurin P, Edeline J, et al. Nivolumab *vs.* sorafenib in advanced hepatocellular carcinoma (CheckMate 459): a randomised, multicentre, open-label, phase 3 trial. Lancet Oncol 2022;23:77–90.

[3] Finn RS, Ryoo BY, Merle P, Kudo M, Bouattour M, Lim HY, et al. Pembrolizumab as second-line therapy in patients with advanced hepatocellular carcinoma in KEYNOTE-240: a randomized, double-blind, phase III trial. J Clin Oncol 2020;38:193–202.

[4] Yau T, Kang Y-K, Kim T-Y, El-Khoueiry AB, Santoro A, Sangro B, et al. Nivolumab (NIVO) + ipilimumab (IPI) combination therapy in patients (pts) with advanced hepatocellular carcinoma (aHCC): results from CheckMate 040. J Clin Oncol 2019;37. 4012–4012.

[5] Finn RS, Qin S, Ikeda M, Galle PR, Ducreux M, Kim TY, et al. Atezolizumab plus bevacizumab in unresectable hepatocellular carcinoma. N Engl J Med 2020;382:1894–1905.

[6] Yofe I, Dahan R, Amit I. Single-cell genomic approaches for developing the next generation of immunotherapies. Nat Med 2020;26:171–177.

[7] **Spitzer MH**, **Carmi Y**, Reticker-Flynn NE, Kwek SS, Madhireddy D, Martins MM, et al. Systemic immunity is required for effective cancer immunotherapy. Cell 2017;168:487–502 e415.

[8] Schneider BJ, Naidoo J, Santomasso BD, Lacchetti C, Adkins S, Anadkat M, et al. Management of immune-related adverse events in patients treated with immune checkpoint inhibitor therapy: ASCO guideline update. J Clin Oncol 2021;39:4073–4126.

[9] Lin D, Lei L, Liu Y, Zhang Y, Hu B, Bao G, et al. Membrane IL1alpha inhibits the development of hepatocellular carcinoma via promoting T- and NK-cell activation. Cancer Res 2016;76:3179–3188.

[10] Chew V, Lai L, Pan L, Lim CJ, Li J, Ong R, et al. Delineation of an immunosuppressive gradient in hepatocellular carcinoma using high-dimensional proteomic and transcriptomic analyses. Proc Natl Acad Sci U S A 2017;114:E5900–E5909.

[11] **Yeo JG**, **Wasser M**, Kumar P, Pan L, Poh SL, Ally F, et al. The Extended Polydimensional Immunome Characterization (EPIC) web-based reference and discovery tool for cytometry data. Nat Biotechnol 2020;38:679–684.

[12] Efremova M, Vento-Tormo M, Teichmann SA, Vento-Tormo R. CellPhoneDB: inferring cell-cell communication from combined expression of multi-subunit ligand-receptor complexes. Nat Protoc 2020;15:1484–1506.

[13] El-Khoueiry AB, Sangro B, Yau T, Crocenzi TS, Kudo M, Hsu C, et al. Nivolumab in patients with advanced hepatocellular carcinoma (CheckMate 040): an open-label, non-comparative, phase 1/2 dose escalation and expansion trial. Lancet 2017;389:2492–2502.

[14] Elliott LA, Doherty GA, Sheahan K, Ryan EJ. Human tumor-infiltrating myeloid cells: phenotypic and functional diversity. Front Immunol 2017;8:86.

[15] Bottcher JP, Bonavita E, Chakravarty P, Blees H, Cabeza-Cabrerizo M, Sammicheli S, et al. NK cells stimulate recruitment of cDC1 into the tumor microenvironment promoting cancer immune control. Cell 2018;172:1022–1037 e1014.

[16] **Liao X**, **Sharma N**, Kapadia F, Zhou G, Lu Y, Hong H, et al. Kruppel-like factor 4 regulates macrophage polarization. J Clin Invest 2011;121:2736–2749.
[17] Daley D, Mani VR, Mohan N, Akkad N, Ochi A, Heindel DW, et al. Dectin 1 activation on macrophages by galectin 9 promotes pancreatic carcinoma and peritumoral immune tolerance. Nat Med 2017;23:556–567.
[18] Gardner A, de Mingo Pulido A, Ruffell B. Dendritic cells and their role in immunotherapy. Front Immunol 2020;11:924.
[19] Viitala M, Virtakoivu R, Tadayon S, Rannikko J, Jalkanen S, Hollmen M. Immunotherapeutic blockade of macrophage clever-1 reactivates the CD8(+) T-cell response against immunosuppressive tumors. Clin Cancer Res 2019;25:3289–3303.
[20] Wolf MJ, Seleznik GM, Zeller N, Heikenwalder M. The unexpected role of lymphotoxin beta receptor signaling in carcinogenesis: from lymphoid tissue formation to liver and prostate cancer development. Oncogene 2010;29:5006–5018.
[21] Wajant H, Siegmund D. TNFR1 and TNFR2 in the control of the Life and death balance of macrophages. Front Cell Dev Biol 2019;7:91.
[22] Han X, Wang Y, Sun J, Tan T, Cai X, Lin P, et al. Role of CXCR3 signaling in response to anti-PD-1 therapy. EBioMedicine 2019;48:169–177.
[23] **Brasseit J**, **Althaus-Steiner E**, Faderl M, Dickgreber N, Saurer L, Genitsch V, et al. CD4 T cells are required for both development and maintenance of disease in a new mouse model of reversible colitis. Mucosal Immunol 2016;9:689–701.
[24] Yan F, Du R, Wei F, Zhao H, Yu J, Wang C, et al. Expression of TNFR2 by regulatory T cells in peripheral blood is correlated with clinical pathology of lung cancer patients. Cancer Immunol Immunother 2015;64:1475–1485.
[25] Sangro B, Sarobe P, Hervas-Stubbs S, Melero I. Advances in immunotherapy for hepatocellular carcinoma. Nat Rev Gastroenterol Hepatol 2021;18:525–543.
[26] Tai D, Choo SP, Chew V. Rationale of immunotherapy in hepatocellular carcinoma and its potential biomarkers. Cancers (Basel) 2019;11.
[27] **Sangro B**, **Melero I**, Wadhawan S, Finn RS, Abou-Alfa GK, Cheng AL, et al. Association of inflammatory biomarkers with clinical outcomes in nivolumab-treated patients with advanced hepatocellular carcinoma. J Hepatol 2020.
[28] **Ma L**, **Hernandez MO**, Zhao Y, Mehta M, Tran B, Kelly M, et al. Tumor cell biodiversity drives microenvironmental reprogramming in liver cancer. Cancer Cell 2019;36:418–430 e416.
[29] Krieg C, Nowicka M, Guglietta S, Schindler S, Hartmann FJ, Weber LM, et al. High-dimensional single-cell analysis predicts response to anti-PD-1 immunotherapy. Nat Med 2018;24:144–153.
[30] Manjarrez-Orduno N, Menard LC, Kansal S, Fischer P, Kakrecha B, Jiang C, et al. Circulating T cell subpopulations correlate with immune responses at the tumor site and clinical response to PD1 inhibition in non-small cell lung cancer. Front Immunol 2018;9:1613.
[31] **Yost KE**, **Satpathy AT**, Wells DK, Qi Y, Wang C, Kageyama R, et al. Clonal replacement of tumor-specific T cells following PD-1 blockade. Nat Med 2019;25:1251–1259.
[32] **Subudhi SK**, **Aparicio A**, Gao J, Zurita AJ, Araujo JC, Logothetis CJ, et al. Clonal expansion of CD8 T cells in the systemic circulation precedes development of ipilimumab-induced toxicities. Proc Natl Acad Sci U S A 2016;113:11919–11924.
[33] **Das R**, **Bar N**, Ferreira M, Newman AM, Zhang L, Bailur JK, et al. Early B cell changes predict autoimmunity following combination immune checkpoint blockade. J Clin Invest 2018;128:715–720.
[34] **Litchfield K**, **Reading JL**, **Puttick C**, Thakkar K, Abbosh C, Bentham R, et al. Meta-analysis of tumor- and T cell-intrinsic mechanisms of sensitization to checkpoint inhibition. Cell 2021;184:596–614 e514.
[35] Perez-Ruiz E, Minute L, Otano I, Alvarez M, Ochoa MC, Belsue V, et al. Prophylactic TNF blockade uncouples efficacy and toxicity in dual CTLA-4 and PD-1 immunotherapy. Nature 2019;569:428–432.
[36] Yang Y, Islam MS, Hu Y, Chen X. TNFR2: role in cancer Immunology and immunotherapy. Immunotargets Ther 2021;10:103–122.
[37] Notley CA, Inglis JJ, Alzabin S, McCann FE, McNamee KE, Williams RO. Blockade of tumor necrosis factor in collagen-induced arthritis reveals a novel immunoregulatory pathway for Th1 and Th17 cells. J Exp Med 2008;205:2491–2497.
[38] Vollmer O, Felten R, Mertz P, Lebrun-Vignes B, Salem JE, Arnaud L. Characterization of auto-immune hepatitis associated with the use of anti-TNFalpha agents: an analysis of 389 cases in VigiBase. Autoimmun Rev 2020;19:102460.